Direct Observation of Ion-Bernstein-Wave-Induced Poloidal Flow in TFTR

B. P. LeBlanc,[1] R. E. Bell,[1] S. Bernabei,[1] J. C. Hosea,[1] R. Majeski,[1] M. Ono,[1] C. K. Phillips,[1]
J. H. Rogers,[2] G. Schilling,[1] C. H. Skinner,[1] and J. R. Wilson[1]

[1]*Princeton Plasma Physics Laboratory, Princeton, New Jersey 08540*
[2]*Intevac, Inc., Santa Clara, California 95054-2704*
(Received 21 September 1998)

Shearing of the plasma poloidal rotation velocity was observed during application of ion Bernstein wave power in the Tokamak Fusion Test Reactor. The first evidence of corroboration between measured poloidal velocity shearing and actively induced Reynolds stress effects is presented. A model reproduces salient experimental features: The observed sheared flow occurs near the tritium fifth harmonic cyclotron resonance layer and depends strongly on the tritium density in agreement with the model. Furthermore, the model reproduces the observed insensitivity of the induced rotation to the tritium density in the region between the third deuterium harmonic layer and the fifth tritium harmonic layer. [S0031-9007(98)08107-1]

The prospect of using externally driven waves to impel plasma motion capable of breaking up the turbulence eddies and thereby reduce transport [1] has renewed interest in ion Bernstein waves (IBW) [2] as a means to control actively transport. These waves are well suited for the task because of their short wavelength—on the order of the ion gyro radius—and strong single-pass localized absorption, when in proximity of an ion resonance. Following the encouraging results obtained on PBX-M [3] with externally launched IBW, an IBW experiment was planned and conducted on the Tokamak Fusion Test Reactor (TFTR) [4], during which sheared poloidal flow was indeed observed. In this Letter, we analyze the experimental data and find it to be in agreement with a model proposed earlier [5], where the wave-induced Reynolds stress drives, in the present case, a spatially sheared poloidal rotation near the fifth tritium ion-cyclotron harmonic layer. Such results have important ramifications for active control of local transport in magnetic fusion devices.

The data presented here pertain to "direct launch" IBW, where we used mode transformation from edge-excited electron plasma waves into ion Bernstein waves as a means to induce IBW in the plasma. For this purpose, a dedicated antenna, with rf current directed in the toroidal direction and comprising two pairs of current elements symmetrically distributed above and below the horizontal midplane was commissioned. Figure 1(a) shows a vertical cross section of the plasma. The magnetic axis, R_0, is at 271 cm, the third harmonic deuterium cyclotron resonance $(3\Omega_D)$ layer at $R_{3\Omega_D} \approx 283$ cm, the fifth harmonic tritium $(5\Omega_T)$ layer at $R_{5\Omega_T} \approx 314$ cm, and the plasma edge R_a at 353 cm. The antenna first surface is at 360 cm. The antenna rf frequency was $\omega = 76$ MHz and the toroidal field at the magnetic axis was 3.44 T.

Selected experimental traces for a discharge with IBW are shown in Fig. 1(b). The bottom panel displays neutral beam and antenna launched powers, along with power radiated by the plasma. The 0.36 MW IBW power is added 1 sec after the onset of the 2.5 MW neutral beam injection (NBI). The top panel shows the perpendicular (diamagnetic) stored energy. The increase associated with IBW, although small compared to the effects of the neutral beam injection, is consistent with the relative power levels. The second panel displays the line integrated density, which also shows an increase during IBW. Although the NBI was deuterium only, the level of deuterium-tritium (DT) neutron emission shown in panel three is indicative of a sizeable tritium fraction among the plasma species. Spectroscopic measurements [6] point to the wall as the tritium source; about 35% of the Balmer-alpha recycling light is of tritium origin. Analysis of the data with TRANSP [7] has shown that a tritium ion density in the low 10^{12} cm^{-3} range had to be invoked to reproduce the DT neutron emission data. A preceding experiment with intensive tritium usage explains the wall condition. As we will see, the amount of tritium has important implications in the data analysis.

A poloidal velocity diagnostic [8] was installed during the last TFTR campaign. Its high throughput and opposing views permitted high precision measurements of the carbon poloidal velocity. Since we are interested in the change in poloidal velocity, Δv_θ, occurring during IBW coupling, we used the following procedure: (1) The data was averaged over the 0.5 sec immediately preceding the application of IBW power; this averaging window occurred after the transient effects associated with the NBI onset had damped away; (2) this averaged profile was then subtracted over the whole time sequence. This procedure has the advantage of removing systematic effects between adjacent spatial channels. We will refer to the incremental change in the carbon poloidal velocity Δv_θ as the flow, and will use the symbol v_θ for the related "nonincremental" poloidal velocity. The data can be seen in Fig. 2(a), where we overlay the Δv_θ time evolution at six major radii. Positive Δv_θ corresponds to the ion-diamagnetic drift direction. In the region of interest $\Delta v_\theta / v_\theta \lesssim 0.3$. It can be seen that, for times prior to the IBW application, $\Delta v_\theta \approx 0$
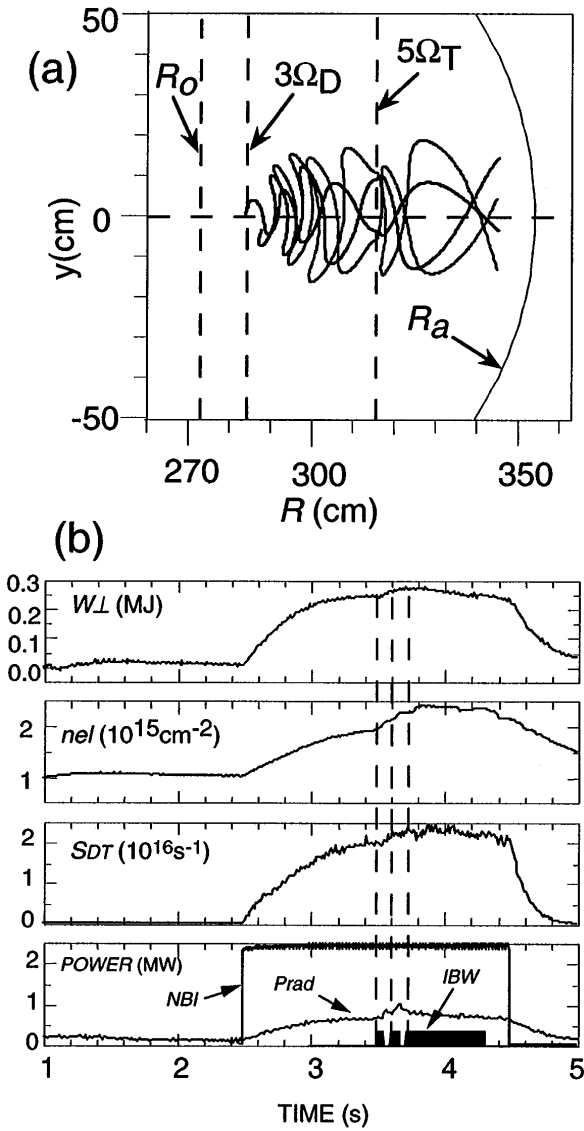
FIG. 1. (a) Vertical cross section showing resonance layer $3\Omega_T$ and $5\Omega_T$ locations, magnetic axis R_0, and outer plasma edge R_a. The trajectories of four rays onto the poloidal plane are also shown. (b) Selected discharge time traces: Stored energy, line-integrated density, DT neutrons, heating, and radiated powers.

with a stable profile, as indicated by little change in the radial direction and a slow negative drift with time. On the other hand, when IBW was applied, rapid and substantial changes occurred, leading to a sheared Δv_θ profile. These modifications are landmarked by the ion-cyclotron layers present in the plasma. Looking at Fig. 2(a), we can see that, while Δv_θ fell to negative values in the $R_{3\Omega_D} < R < R_{5\Omega_T}$ region, it actually grew positive in the $R_{5\Omega_T}$ vicinity, where the peak value occurs. In comparison, we can see in Fig. 2(b) results obtained when this same analysis procedure is applied to a reference "no-IBW" discharge. In this case, there is only a small change in the Δv_θ profile, consistent with the slow drift mentioned above.

The presence of a negative flow in the $R_{3\Omega_D} < R < R_{5\Omega_T}$ region is a persistent feature of the experimental data,
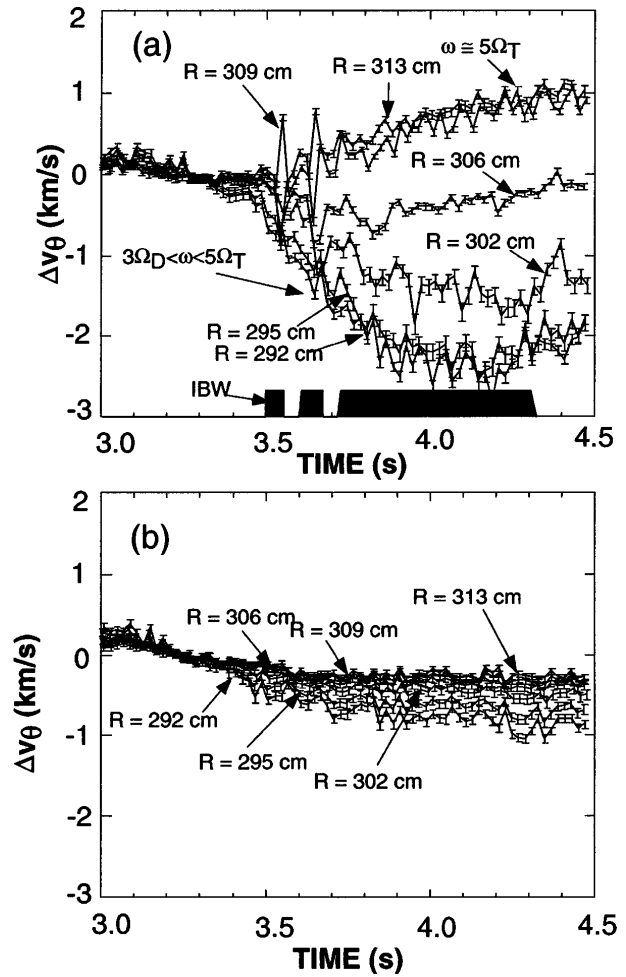

FIG. 2. Experimental carbon Δv_θ at six major radius locations during (a) discharge with IBW power; (b) discharge without IBW power.

although one should keep in mind that the database for these conditions comprises only a handful of discharges. On the other hand, the driven flow in $R_{5\Omega_T}$ vicinity appears to depend on the tritium concentration. Figure 3 illustrates
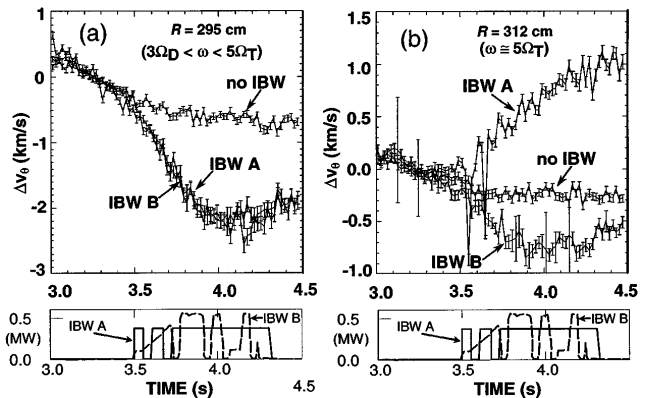

FIG. 3. Overlay of Δv_θ time evolution for IBW discharges IBW A (higher tritium density) and IBW B (lower tritium density), and for a no-IBW discharge: (a) at $R = 295$ cm; (b) at $R = 312$ cm.
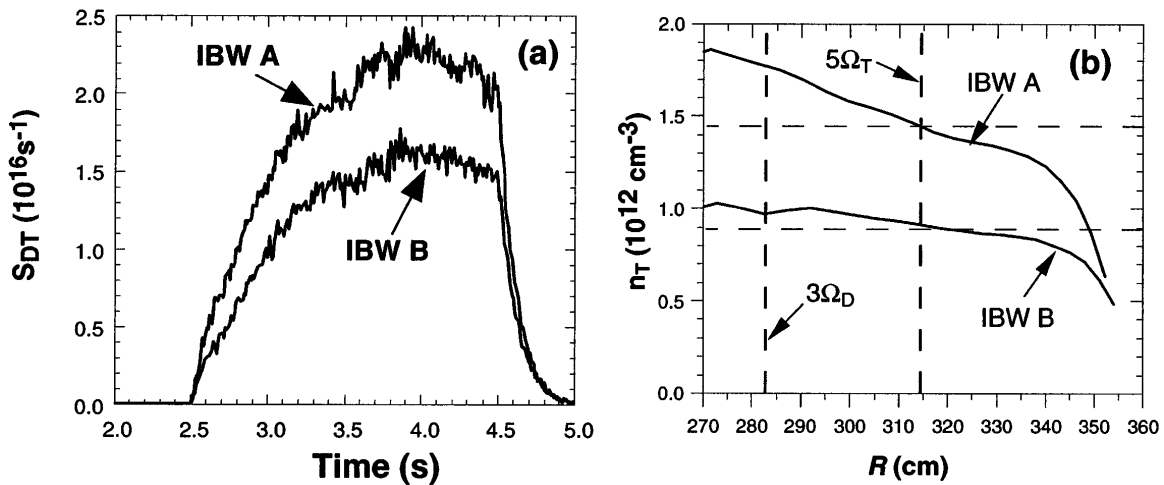
FIG. 4. Comparison between discharges IBW *A* and IBW *B*: (a) DT neutron source strength temporal evolutions; (b) TRANSP evaluation of n_T at $t \cong 4$ s.

this effect, where we overlay temporal evolution of Δv_θ data from three discharges. Discharges labeled "IBW *A*" and "no-IBW" correspond to the two cases presented above. Discharge "IBW *B*" had a significantly lower tritium density than IBW *A*; estimates of the tritium density levels follow. Looking at Fig. 3(a), we see that between the $3\Omega_D$ and $5\Omega_T$ layers, at $R \approx 295$ cm, both IBW *A* and IBW *B* discharges have a similar behavior, namely, that of a negative poloidal flow compared to the no-IBW case. On the other hand, IBW *A* and IBW *B* behave differently at $R = 312$ cm, near the $5\Omega_T$ layer. While IBW *A* shows a positive flow reaching 1 km/s, IBW *B* features a negative flow, falling to -0.8 km/s.

Quantitative statements can be made about the tritium density, n_T, in plasmas IBW *A* and IBW *B*. In these discharges, where the NBI is done with deuterium, the strength of the neutron emission generated by the DT nuclear reactions is sensitive to the level of the tritium ion density in the core region of the target plasma. Figure 4(a) gives the temporal evolution of the experimental DT neutron production; the DT neutron rate for IBW *A* was 40% higher than for IBW *B*. We made use of the DT neutron data and of the edge recycling measurement mentioned above to provide constraints for the core and edge tritium density in TRANSP analyses, and extract n_T profiles. In Fig. 4(b), we overlay n_T obtained from TRANSP for these two discharges at time $t \approx 3.9$–4.0 s. Near the $5\Omega_T$ layer location, n_T for IBW *A* exceeded that of IBW *B* by 50%. The change in n_T was caused by the progressive wall cleaning during successive discharges; IBW *B* occurred four discharges after IBW *A*.

A ray-tracing code (IBWTRACER) has been developed to analyze the data. The original ray-tracing package, written by Ono [9], has been upgraded to multispecies profiles extracted from TRANSP analyses [10], and models the kinetic resonance structure as described below. We typically use five or six ion species including H, D, T,

a carbonlike impurity, and fast ions during NBI. Each species has its own density profile. The thermal ions are all assumed to have the same temperature profile. After computing the dispersion relation, fans of rays—typically 40 rays are used—with a spectrum characteristic of the antenna are launched. The IBW power deposition is computed (and stored) locally on a spatial grid for each species (electrons, H, D, T, fast D, and C) as the rays are traced. The results from individual rays are summed to obtain the local power deposition and Reynolds stress for each species. A subroutine of the ray-tracing software calculates the induced poloidal velocity Δv_θ using the equation

$$\rho \langle \tilde{v} \cdot \nabla \tilde{v}_\theta \rangle + \mu_{\text{neo}} \times \Delta v_\theta = 0, \qquad (1)$$

where the first term of the left-hand side (LHS) corresponds to the Reynolds stress induced by the IBW [5] and μ_{neo} is the neoclassical viscosity. For these calculations, we used a μ_{neo} formulation by Chang [11]. The second term of the LHS is usually written with brackets around Δv_θ, but these were left out to remain consistent with the above notation where Δv_θ is a guiding-center average.
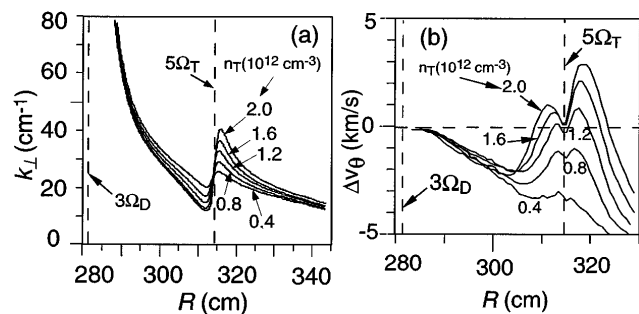

FIG. 5. IBWTRACER predictions over n_T range $(0.4$–$2.0) \times 10^{12}$ cm^{-3}: (a) Real part of the dispersion relation; (b) IBW poloidal drive Δv_θ.

TABLE I. Comparison of computed poloidal driven flow with measurements.

Discharge	IBW A (high n_T)		IBW B (low n_T)	
R (cm)	295 $(R_{3\Omega_D} < R < R_{5\Omega_T})$	314 $(R \approx R_{5\Omega_T})$	295 $(R_{3\Omega_D} < R < R_{5\Omega_T})$	314 $(R \approx R_{5\Omega_T})$
Δv_θ (km/s) Experimental	-2.1 ± 0.1	$+0.7 \pm 0.1$	-2.1 ± 0.1	-0.8 ± 0.1
Δv_θ (km/s) IBWTRACER	-1.25	$+0.6$	-1.25	-1.3

We used IBWTRACER to investigate the theoretical dependence of Δv_θ on n_T. Figure 5 presents predictions obtained for n_T ranging from 0.4×10^{12} to 2.0×10^{12} cm^{-3} near the $5\Omega_T$ layer. In Fig. 5(a), we see that, as n_T increases, the dispersion develops a localized gradient around the $5\Omega_T$ resonance layer. In order to treat the $5\Omega_T$ resonance in a numerically tractable yet accurate manner, the Z-function approximation used in IBWTRACER to compute the real part of the dispersion relation was supplemented in order to achieve proper asymptotic behavior for $|\delta\omega/k_\parallel| \ll v_T$ and for $|\delta\omega/k_\parallel| \gg v_T$, where $\delta\omega = \omega - 5\Omega_T$, $k_\parallel$ is the parallel wave number, and v_T is the tritium thermal velocity. The usual kinetic damping terms with collisional modifications were used for the imaginary part [9]. Making use of Eq. (1), which is applicable for each plasma species, we graph the predicted Δv_θ for carbon in Fig. 5(b). The predicted driven flow is negative and insensitive to n_T at $R \cong 295$ cm, as observed in Fig. 3(a). On the other hand, the predicted Δv_θ in the vicinity of the $5\Omega_T$ layer, $R \approx 314$ cm, varies strongly with n_T, from negative to positive values, in accordance with the experimental observation. For discharge IBW A where $n_T \cong 1.4 \times 10^{12}$ cm^{-3}, one predicts a positive flow around 0.7 km/s, while for IBW B where $n_T \cong 0.9 \times 10^{12}$ cm^{-3}, one gets a negative flow at -1.3 km/sec. The results, computed for time $t \cong 3.9-4.0$ s, are compared in Table I for discharges IBW A and IBW B. It is noteworthy that these calculations, while not including spatial poloidal momentum diffusive effects, are nevertheless able to reproduce correctly the sign of Δv_θ and to match the experimental data within roughly 50%. It should be pointed out here that, by using the "before IBW" subtraction procedure, we have isolated effects related to IBW-induced Reynolds stress, but also removed from consideration effects associated with neutral beam injection. Within the experimental uncertainty the toroidal velocity does not change during the IBW pulse, and pressure gradient effects are not believed to play an important role in the present case.

The IBW ray-tracing model provides satisfactory agreement with salient features of the experimental data. First, the model explains the existence and n_T dependency of the observed Δv_θ near the $5\Omega_T$ layer. Second, the model reproduces the negative Δv_θ observed in the $R_{3\Omega_D} < R < R_{5\Omega_T}$ region and explains its insensitivity to changes in the tritium density. The applicability of the IBW ray-tracing calculation stems from the fact that, in the present case, the induced poloidal flow is small compared to relevant quantities such as the local sound speed and the wave group velocity. The local Mach number (ratio of poloidal velocity v_θ to the acoustic speed) is only about 2%–3%.

The present analysis provides the first evidence of corroboration between measured poloidal velocity shearing and induced Reynolds stress. The ability to reproduce the Δv_θ behavior in space and with different tritium density gives credence to the model, and supports IBW-induced Reynolds stress as the origin of the poloidal drive observed on TFTR. Finally, the choice of harmonic ($5\Omega_T$ in the present case) was dictated by hardware considerations and TFTR's mission to investigate DT plasmas, but other harmonics should work as well.

[1] C. G. Craddock and P. H. Diamond, Phys. Rev. Lett. **67**, 1536 (1991).

[2] H. Biglari et al., in Radio Frequency Power in Plasmas, edited by Donald B. Batchelor, AIP Conf. Proc. No. 244 (AIP, New York, 1991), p. 376.

[3] B. P. LeBlanc et al., Phys. Plasmas **2**, 741 (1995).

[4] J. R. Wilson et al., Phys. Plasmas **5**, 1721 (1998).

[5] M. Ono et al., in Proceedings of the Fifteenth International Conference on Plasma Physics and Controlled Nuclear Fusion Research (IAEA, Vienna, 1995), Vol. I, p. 469.

[6] C. H. Skinner et al., Nucl. Fusion **35**, 143–151 (1995).

[7] J. Ongena, M. Evrard, and D. McCune, Fusion Technol. **33**, 181–191 (1998).

[8] R. E. Bell, Rev. Sci. Instrum. **68**, 1273 (1997); R. E. Bell et al., Rev. Sci. Instrum. (to be published).

[9] M. Ono, Phys. Fluids B **5**, 241 (1993).

[10] B. P. LeBlanc, in Radio Frequency Power in Plasmas, edited by Donald B. Batchelor, AIP Conf. Proc. No. 403 (AIP, New York, 1997), p. 73.

[11] C. S. Chang, Phys. Fluids B **5**, 4360 (1993).